Compound drought stressors drive vegetation decline in the African Great Lakes region: a multiscale causal analysis

ENVIRONMENTAL RESEARCH
CLIMATE

PAPER

OPEN ACCESS

RECEIVED
3 November 2025

REVISED
16 January 2026

ACCEPTED FOR PUBLICATION
3 March 2026

PUBLISHED
23 March 2026

Compound drought stressors drive vegetation decline in the African Great Lakes region: a multiscale causal analysis

Pacifique Batungwanayo[1,*], **Marnik Vanclooster**[1] and **Athanase Nkunzimana**[2]

[1] Université Catholique de Louvain, Earth and Life Institute, Croix du Sud 2, Box 2, 1348 Louvain-la-Neuve, Belgium
[2] Centre for Research and Studies on Development in Reconstructing Societies, University of Burundi, UNESCO Avenue No. 2, PO Box 5142, Bujumbura, Burundi
[*] Author to whom any correspondence should be addressed.

E-mail: pbatungwanayo@gmail.com

Keywords: spatiotemporal analysis, vegetation productivity, African Great Lakes region, multiscale causal discovery, teleconnections

Supplementary material for this article is available online

Abstract

Compound hydroclimatic stresses are increasingly threatening vegetation and food security in data-scarce regions like the African Great Lakes region (AGLR). Yet, their effects on vegetation are poorly quantified, limiting the development of effective drought response and food security policies. This study aims to identify the direct drivers and causal pathways of compound drought impacts on vegetation productivity across the region. To address this, this study conducted a comprehensive 25 year analysis (2000–2024) integrating satellite-derived normalized difference vegetation index with key hydroclimatic variables, including precipitation, temperature, soil moisture (SM), vapor pressure deficit (VPD), and teleconnections. Using a wavelet-based causal discovery Peter and Clark momentary conditional independence framework, we move beyond correlation to identify the direct drivers of vegetation stress. Our analysis reveals that croplands and shrublands experienced a 15% greater decline in greenness compared to forests during major climate events, such as the 2015–16 El Niño and the 2023–24 positive Indian Ocean Dipole. Importantly, the causal framework demonstrates that this severe vegetation stress is not primarily driven by precipitation or temperature anomalies alone. Instead, it is causally linked to the combined influence of coinciding VPD and SM deficits. This study provides clear, data-driven evidence that the combined effects of high atmospheric dryness and low SM are linked to significant vegetation productivity loss across the AGLR. These findings provide a scientific foundation for urgently integrating compound VPD-SM metrics into regional drought early-warning systems to improve the lead time and accuracy of food security interventions in the AGLR and similar climate-vulnerable regions.

1. Introduction

Vegetation productivity is essential for carbon storage, water regulation, and food security. These functions are particularly sensitive to climate stressors (Pettorelli *et al* 2005, Ding *et al* 2024, Kooistra *et al* 2024). Long-term monitoring of vegetation dynamics is therefore essential for understanding ecosystem responses to climate variability and human pressures, especially under accelerating global change (Hodgkins *et al* 2025). Satellite remote sensing has transformed this monitoring, with the normalized difference vegetation index (NDVI) enabling the consistent detection of changes in vegetation greenness across broad spatial and temporal scales (Tucker 1979, Pettorelli *et al* 2005). For this study, we define greenness as the satellite-derived NDVI signal, which serves as a practical proxy for photosynthetically active green biomass. Sustained declines in greenness (negative NDVI anomalies) are interpreted here as an indicator of vegetation stress, a condition that can reduce the fundamental ecosystem process of productivity (i.e. the rate of carbon assimilation and biomass accumulation).

Global vegetation patterns are shaped by the complex interplay among climate drivers, land-use change, and ecological feedbacks (Bastos *et al* 2020). While some regions have experienced greening, some tropical and subtropical areas are increasingly showing signs of browning linked to deforestation, agricultural expansion, and recurrent droughts (Wessels *et al* 2012, Zhu *et al* 2016). This trend is particularly concerning in low-latitude regions where data are often scarce despite their high vulnerability to climate extremes. In Africa, where over 60% of the population relies on rain-fed agriculture, the ecological and socioeconomic stakes of climate extremes are particularly high (FAO 2022).

The African Great Lakes region (AGLR) is a crucial global hotspot for studying climate-vegetation interactions, offering a confluence of unique characteristics: it is a tropical montane region with high climate sensitivity; its climate is governed by a complex interplay of multiple teleconnections; it hosts a high-density, rain-fed agricultural population; and it features a rapidly changing landscape mosaic of forests, shrublands, and croplands. The region hosts rich biodiversity and essential freshwater resources (Singh *et al* 2006, Du *et al* 2023, Plisnier *et al* 2023) but faces mounting pressures from population growth, land degradation, and climate variability (Funk *et al* 2015). The region's climate is strongly influenced by global teleconnections, such as the El Niño-Southern Oscillation (ENSO) and the Indian Ocean Dipole (IOD), which modulate rainfall and temperature patterns (Batungwanayo *et al* 2024, Zita *et al* 2025). However, the full impact of these hydroclimatic disruptions on the region's diverse ecosystems remains unclear. ENSO-induced anomalies influence rainfall and temperature patterns unevenly: western sectors such as Sudan, South Sudan, and northern Uganda often suffer droughts during El Niño years, while eastern regions like Somalia, southeastern Ethiopia, and coastal Kenya frequently experience flooding (MacLeod and Caminade 2019, Cook *et al* 2024).

These hydroclimatic disruptions modify soil moisture (SM), evapotranspiration, and photosynthetic activity-leading potentially to modifications in vegetation productivity (Cook *et al* 2024). In the Great Lakes subregion, particularly Burundi, Rwanda, Uganda, and western Kenya, ENSO events elevate ecosystem stress through intensified aridity and heat. Concurrent positive IOD phases can exacerbate rainfall extremes by enhancing convective activity in East Africa (Blau and Ha 2020, Ingeri *et al* 2024). Major ENSO events (1997/98, 2015/16, and 2023/24) provide valuable case studies for assessing vegetation responses to climate extremes (Raghuraman *et al* 2024). Rainfall in the region follows bimodal seasonality (March–May, October–December), shaped by Walker circulation, ENSO, and IOD dynamics (Dunning *et al* 2016, Nicholson 2017). Positive IOD events generate a sea surface temperature gradient that enhances rainfall across Eastern Africa, particularly in southern and eastern sectors (Thielke and Mölg 2019, Blau and Ha 2020). In addition, local factors such as orographic effects from the Kivu Rift and Rwenzori Mountains, as well as convection over Lake Victoria, interact with these global drivers to influence vegetation dynamics (Sato and Ise 2012, De Keersmaecker *et al* 2015, Rahimabadi and Azarnivand 2023).

Vegetation productivity is a complex physiological response to a suite of interrelated hydroclimatic factors, extending beyond rainfall anomalies alone. These include not only precipitation amount and frequency but also surface temperature, SM availability, and atmospheric dryness, a key measure of which is vapor pressure deficit (VPD). Elevated temperatures and high VPD increase plant water stress by promoting stomatal closure, which ultimately reduces photosynthetic activity (Grossiord *et al* 2020). This compound phenomenon, often referred to as a 'hot drought' (the simultaneous occurrence of drought and heatwaves that synergistically amplifies impacts), can be more detrimental to plant health than a lack of rainfall alone (Bevacqua *et al* 2023, Wright 2024, Mondal and Vivoni 2025). Meanwhile, declining SM can directly constrain vegetation activity, particularly in semi-humid and drought-prone zones (Humphrey *et al* 2021). These factors interact synergistically with climate modes like ENSO to amplify vegetation stress (Nicholson 2014, Cordeiro *et al* 2021).

However, the causal pathways through which these compound stressors-particularly the interplay between VPD and SM-impact vegetation greenness and productivity across different temporal scales and climate phases remain inadequately understood. Most studies rely on correlations, failing to disentangle direct drivers from indirect feedbacks. Furthermore, the role of land cover in mediating these responses is not fully quantified.

To address this critical knowledge gap, we present a comprehensive spatiotemporal analysis of vegetation dynamics across the AGLR over a 25 year period (2000–2024), a climate-sensitive tropical system influenced by large-scale teleconnections and dominated by rain-fed ecosystems. By integrating NDVI-derived greenness with multi-source environmental data, we aim to: (i) quantify the relative impacts of compound hydroclimatic extremes (high VPD + low SM) versus precipitation deficits on vegetation greenness and inferred stress, (ii) evaluate how land cover type modulates ecosystem resilience and recovery times from drought stress, and (iii) identify the phase-locked and scale-dependent causal pathways by which global teleconnections (ENSO, IOD) and local hydroclimate variables drive vegetation

dynamics. To the best of our knowledge, no previous study has examined the causal interactive effects of multiple climate drivers on vegetation in the AGLR at these temporal scales. Our findings offer critical insights into ecosystem responses in this highly vulnerable region, with important implications for sustainable land management, climate change adaptation, and regional development planning.

2. Materials and methods

2.1. Study area

This study focuses on the AGLR, a transboundary zone spanning parts of East and Central Africa, encompassing Burundi, Rwanda, Uganda, Kenya, Tanzania, and the eastern Democratic Republic of Congo (DRC). The region hosts several large freshwater lakes, most notably Lake Victoria, Lake Tanganyika, and Lake Albert, and is recognized as both a biodiversity hotspot and a climate-sensitive area (Haile *et al* 2019). Geographically, the AGLR extends from approximately 12 °S to 5 °N latitude and 20 °E to 45 °E longitude (figure 1(a)), encompassing a wide topographic gradient from lowland basins ($<$467 m) to highland plateaus ($>$ 2533 m). Rift Valley escarpments and volcanic highlands dominate the landscape, creating distinct agroecological zones and microclimates that shape land use, vegetation distribution, and agricultural potential (Kayiranga *et al* 2022).

The region exhibits heterogeneous land cover, as depicted in the ESA land use and land cover Map for 2021 (figure 1(b)). Forests dominate parts of eastern DRC and Uganda, while shrublands and croplands prevail in Burundi, Rwanda, and portions of Kenya and Tanzania. Wetlands and built-up areas are interspersed across the region. This mosaic of land cover types underscores the dynamic interplay between natural ecosystems and human activities (Zhou *et al* 2014). Vegetation dynamics, assessed via the NDVI, further highlight spatial variability: high NDVI values ($\geqslant 0.7$) correspond to dense forests and perennial vegetation, while lower values (<0.3) characterize croplands and sparsely vegetated zones (figure 1(c)). Areas with high NDVI standard deviation (figure 1(d)), such as around Lake Victoria and northern Tanzania, reflect pronounced seasonal fluctuations, highlighting vegetation-climate sensitivity (Xu *et al* 2024).

The AGLR's combination of complex topography, high dependence on rain-fed agriculture, and exposure to multi-scale climate variability (e.g. ENSO, IOD) makes it particularly vulnerable to climate change impacts. These characteristics also make it an ideal natural laboratory for investigating climate-vegetation interactions and identifying resilience pathways.

2.2. Data sources

To investigate vegetation dynamics across the AGLR, this study uses a compiled multi-source dataset integrating satellite-derived vegetation indices, local hydroclimatic variables, and large-scale climate oscillation indicators (see table 1). Vegetation productivity is assessed using the NDVI, obtained from the MODIS MOD13Q1 Version 6.1 product, which provides 16 day composite data at a spatial resolution of 250 m. The NDVI time series, retrieved from the Google Earth Engine platform, are aggregated to a monthly scale and spatially averaged across the entire AGLR study area. This produced a single regional NDVI time series, which was used for the analysis to identify the dominant climate-vegetation mechanisms at the regional scale. NDVI serves as a robust proxy for monitoring vegetation health and productivity across diverse landscapes (Pettorelli *et al* 2005, Assis *et al* 2024).

Key hydroclimatic drivers of vegetation variability are derived from the ERA5-Land reanalysis dataset (Muñoz Sabater *et al* 2021). The selected variables include monthly Precipitation (P), near-surface Temperature (T), VPD, and SM in the upper 100 cm of soil. These variables were similarly spatially averaged to produce corresponding regional monthly time series. They are recognized as critical for influencing vegetation processes such as photosynthesis, evapotranspiration, and plant water stress. Their high temporal resolution and spatial consistency enable detailed analysis of climate-vegetation interactions at the regional scale.

Land use classification for stratified analysis is based on the ESA WorldCover 2021 product. The 'cropland' class was analyzed as a single entity. This approach is justified for a regional-scale study as the AGLR's agricultural landscape is overwhelmingly dominated by smallholder, rain-fed systems. Areas equipped for irrigation constitute a minor and spatially limited fraction of the total cropland extent (Nhamo *et al* 2024, Sogno *et al* 2024); therefore, the aggregated vegetation-climate signal for this class is representative of the region's predominant rain-fed agricultural vulnerability.

To account for the influence of large-scale climate patterns, the study includes two major climate drivers: the oceanic Niño index (ONI) and the dipole mode index (DMI). The ONI is widely used to characterize ENSO events and is calculated as a 3 month running mean of sea surface temperature (SST) anomalies in the Niño 3.4 region (5 °N–5 °S, 170 °W–120 °W) of the eastern Pacific Ocean. El Niño or

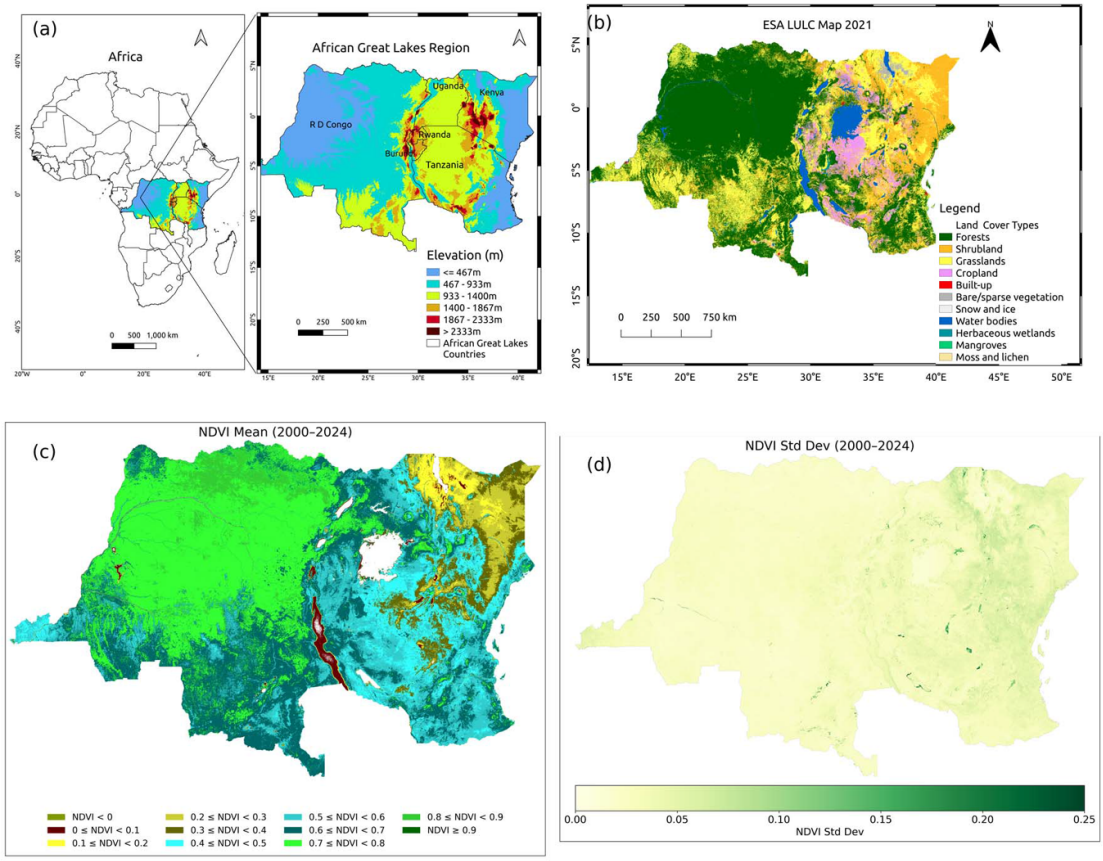

Figure 1. Study area and vegetation characteristics of the African Great Lakes region: (a) Location and elevation of the AGLR within Africa. (b) ESA WorldCover 2021 land use/land cover map showing major land cover types. (c) Mean NDVI (2000–2024) indicating spatial patterns of vegetation productivity. (d) NDVI standard deviation (2000–2024) reflecting vegetation variability over time.

Table 1. Overview of datasets used in the study.

Variable	Description	Source	Spatial resolution	Temporal span	References
Precipitation	Rainfall measurements	CHIRPS	5 km	Monthly	Funk *et al* (2015)
Temperature	Air temperature	ERA5-Land	9 km	Monthly	Muñoz Sabater (2019)
VPD	Vapor pressure deficit	ERA5-Land	9 km	Monthly	Muñoz Sabater (2019)
SM	Soil moisture	ERA5-Land	9 km	Monthly	Muñoz Sabater (2019)
NDVI	Normalized difference vegetation index	MODIS	250 m	16 days	Didan (2021)
ENSO	El-Niño Southern Oscillation			Monthly	https://origin.cpc.ncep.noaa.gov/products/analysis_monitoring/ensostuff/ONI_v5.php
DMI	Dipole mode index			Monthly	https://psl.noaa.gov/gcos_wgsp/Timeseries/Data/dmi.had.long.data

La Niña events are typically defined when the ONI exceeds ± 0.5 °C for at least five consecutive overlapping 3 month periods. The DMI quantifies the strength of the IOD based on the SST gradient between the western (50 °E–70 °E, 10 °S–10 °N) and southeastern (90 °E–110 °E, 10 °S–0 °N) equatorial Indian Ocean. Positive and negative DMI values respectively indicate the positive and negative phases of the IOD, each associated with distinct impacts on rainfall variability in the East African region (Saji *et al* 1999, Nicholson 2017).

By integrating these local and remote drivers, the dataset provides a solid foundation for assessing vegetation responses to both regional hydroclimatic variability and broader modes of climate variability.

Table 2. Categories of dry and wet conditions based on SPI values following McKee *et al* (1993).

SPI value	Category
$\geqslant 2.00$	Extremely wet
1.50 to 1.99	Severely wet
1.00 to 1.49	Moderately wet
−0.99 to 0.99	Near normal
−1.49 to −1.00	Moderately dry
−1.99 to −1.50	Severely dry
$\leqslant -2.00$	Extremely dry

2.3. Analytical approach

We employed a multi-stage analytical framework to first characterize drought patterns, then assess correlations, and finally uncover causal relationships across different climate phases and temporal scales.

2.3.1. Standardized precipitation index (SPI)

The SPI is a widely used meteorological drought indicator that measures precipitation anomalies over specified time scales (McKee *et al* 1993). In this study, we downscaled the two decades of monthly precipitation records spanning from 2000 to 2024 at 1 km resolution to compute the 3 month SPI values across the AGLR. The long-term rainfall data was fitted to a Gamma probability distribution to convert moisture deviations into standardized normal values which allowed for consistent drought assessment. We applied the World Meteorological Organization's thresholds (McKee *et al* 1993) to classify drought severity (see table 2).

2.3.2. Correlation analysis

We used both Pearson and Spearman correlation coefficients to assess bivariate associations between hydroclimatic drivers and vegetation productivity. Pearson correlation measures linear relationships under the assumption of normally distributed variables, whereas Spearman correlation, based on ranked data, is robust to non-linear trends and outliers (Wilks 2011). Employing both metrics provides complementary perspectives on potential dependencies.

2.3.3. Phase-based causal discovery

To assess how large-scale ocean-atmosphere modes modulate causal relationships among environmental variables, we implemented a phase-based causal discovery framework. The study period was classified into ENSO (El Niño, La Niña, Neutral) and IOD (positive, negative, neutral) phases using ONI and DMI thresholds (Bamston *et al* 1997, Saji *et al* 1999). A full list of the classified events is provided in Supplementary table S1. For each phase or phase combination (e.g. El Niño-Positive IOD), all occurrences during the study period were concatenated to form composite time series of the key variables (T, P, VPD, SM, NDVI). Transitional periods not meeting the threshold criteria were excluded to avoid phase ambiguity. Although this approach removes temporal continuity across phases, it enables the identification of phase-specific causal structures while ensuring sufficient sample size and stationarity.

Causal networks were inferred using the PCMCI (Peter and Clark momentary conditional independence) algorithm (Runge *et al* 2019), a state-of-the-art, constraint-based method for time series data. PCMCI identifies links by rigorously testing for conditional independence among variables across multiple time lags, controlling for common causes and false discoveries. A directed causal link (e.g. $SM_{t-\tau} \rightarrow NDVI_t$) is inferred when the past state of one variable provides statistically unique information for predicting another, conditional on the entire observed system. This identifies dominant time-asymmetric dependencies within the coupled climate-vegetation system. It is important to note that in systems with strong bidirectional feedbacks (e.g. between SM and NDVI), such links represent the net temporal signature of these interactions at the analyzed monthly resolution, rather than proof of a unidirectional mechanistic driver. We used partial correlation conditional independence tests, with a maximum time lag of six months ($\tau_{max} = 6$) and a significance threshold of $\alpha = 0.05$.

This approach enabled us to reveal phase-specific causal pathways and determine how vegetation responses shift under different climate regimes. To specifically assess the standalone influence of the IOD, we also conducted separate analyses focusing on positive IOD (DMI $\geqslant$ 0.4) and negative IOD (DMI $\leqslant$ −0.4) phases, regardless of concurrent ENSO activity. Due to the limited number of observations in the subsets, the combinations of ENSO and IOD phases were not taking into account.

2.3.4. Multiscale causal discovery via wavelet decomposition

To capture the scale-dependent nature of climate-vegetation interactions, we integrated wavelet decomposition with causal inference. Monthly time series spanning 25 years were decomposed using the maximal overlap discrete wavelet transform with a Daubechies 4 ('db4') mother wavelet. The db4 wavelet is a standard choice for geophysical time series analysis due to its compact support and suitability for representing both smooth trends and localized variations in non-stationary climate data (Percival and Walden 2000).

A maximum decomposition level of $J = 6$ was chosen. This parameter determines the range of temporal scales isolated from the original signal. The resulting six sets of wavelet detail coefficients $(D_1, D_2, \cdots, D_6)$ and one set of approximation coefficients (A_6) correspond to distinct frequency bands. The characteristic period τ_j (in months) associated with each detail level j for a monthly time series (sampling interval $\Delta_t = 1$ month) is governed by the relationship $\tau_j \approx 2^j \cdot \Delta_t \cdot C_\psi$, where C_ψ is a wavelet-specific constant approximately equal to 1.0 for the db4 wavelet (Torrence and Compo 1998). Consequently, setting $J = 6$ yields the following scale-specific series: D_1 captures variability at periods of ∼2–4 months (sub-seasonal, rapid vegetation responses), D_2 at ∼4–8 months (seasonal cycles, e.g. bimodal rainy seasons), D_3 at ∼8–16 months (semi-annual to annual variability), D_4 at ∼16–32 months (interannual, capturing the quasi-biennial component of ENSO), D_5 at ∼32–64 months (interannual to multi-year, encompassing the full 2–5 year ENSO/IOD band), and D_6 at ∼64–128 months (multi-year to decadal trends). This range was explicitly chosen to span the complete hierarchy of processes relevant to AGLR ecosystem dynamics, from short-term physiological stress to the low-frequency forcing of major climate teleconnections (Nicholson 2017, Küllahcı and Altunkaynak 2024). The final approximation series, A_6, represents the residual trend at scales longer than 128 months.

For each decomposition level j, reconstructed time series were detrended and aligned across variables before causal inference using PCMCI, with parameters matching the phase-based analysis ($\tau_{\max} =$ 6 months, $\alpha = 0.05$). This multiscale approach enabled the detection of frequency-specific causal drivers, revealing the temporal complexity of drought-vegetation linkages.

3. Results

3.1. Correlational relationships between climate variables and vegetation

We first assessed the linear and monotonic associations between the principal hydroclimatic variables and vegetation greenness (NDVI). The correlation matrix (figure S2) revealed consistent and significant relationships across both Pearson and Spearman coefficients. NDVI exhibited a strong positive correlation with SM and a strong negative correlation with VPD. Precipitation was positively correlated with NDVI and SM, and negatively with VPD. These robust associations confirmed the intertwined nature of these variables and provided the foundation for a more detailed causal analysis.

3.2. Co-evolution of vegetation productivity and drought indicators

The AGLR exhibits marked spatial heterogeneity in vegetation cover, shaped by intra-seasonal to interannual fluctuations in hydroclimatic conditions. This variability is mainly controlled by regional meteorological dynamics and influenced by large-scale climate teleconnections. Vegetation productivity is therefore the result of interacting proximal (precipitation, SM, VPD) and remote (ENSO, IOD) influences acting across multiple temporal scales.

To understand these dynamics, we analyzed time series of standardized NDVI anomalies and the SPI-3 (figure 2(a)), alongside ONI and DMI (figure 2(b)) from 2000 to 2024. This co-evolutionary analysis highlights the complex relationship between vegetation health, meteorological drought conditions, and climate teleconnections. Standardized NDVI values below −1 are referred to low NDVI events. During the study period, the low NDVI occurrence has been at intra-annual frequency with severe observed in years 2004, 2006, 2015, 2016, 2019, 2021, 2022, 2023, and 2024 (figure S1 in supporting information. These episodes consistently coincided with negative SPI-3 (meteorological drought), low SM, and elevated VPD (figure 3).

The joint evolution of SPI-3 and NDVI confirms that 3 month rainfall deficits (SPI-3 < -1) systematically trigger vegetation decline. Drought years such as 2005–2006, 2010–2011, 2015–2016, and 2023–2024 all exhibit both significant negative SPI anomalies and sharp NDVI reductions. While this consistent pattern highlights the damaging effects of climate stress on ecosystems, NDVI responses vary in magnitude, suggesting that ecosystem resilience, land cover type, and drought duration may buffer impacts in some areas.

Large-scale teleconnections magnify these stresses. ENSO, in particular, has emerged as the dominant remote driver of vegetation dynamics in the AGLR. The strong El Niño of 2015–2016 triggered one

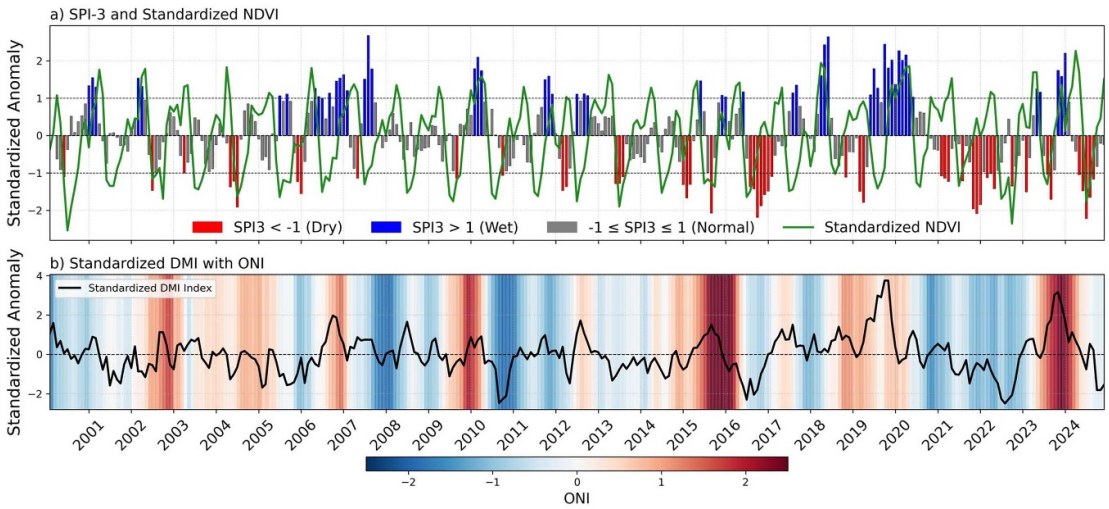

Figure 2. (a) Time series of NDVI with SPI-3 plotted for 2000–2024. A 3 month moving average is applied to smooth the NDVI signal. Colored bars represent meteorological conditions: blue for moderate to severe wet events, red for moderate to severe droughts, and gray for normal periods. (b) ONI as a surface plot for 2000–2024, along with the DMI shown as a black line. The accompanying color scale reflects ONI intensity: red hues denote positive ONI phases (El Niño-like), while blue hues indicate negative phases (La Niña-like).

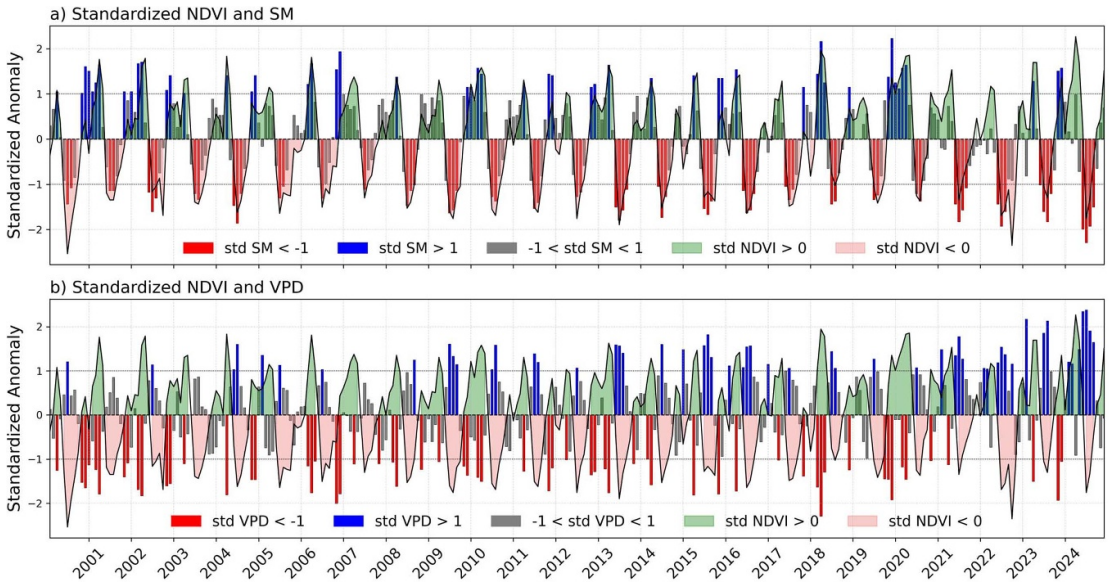

Figure 3. Annual NDVI anomalies overlaid with SM and VPD show that vegetation declines coincide with compound stress from soil and atmospheric water deficits.

of the most severe and spatially extensive droughts of the past two decades, producing persistent NDVI declines across Burundi, Uganda, and Tanzania. Independent studies confirm that ENSO-driven precipitation variability is a primary source of interannual vegetation fluctuations in East Africa (Fer *et al* 2017, Anyamba *et al* 2018). While El Niño events tend to produce drier conditions in southern Africa and wetter anomalies in equatorial East Africa, the AGLR lies at a transitional zone, making it particularly sensitive to compound drought stress. The 2015–2016 case is illustrative: vegetation losses did not recover to pre-event levels even two years later, indicating long-lasting ecosystem impacts (Liu *et al* 2017, Wigneron *et al* 2020).

3.3. SM and atmospheric dryness as dual stressors

Figure 3 illustrates the standardized anomalies of NDVI relative to two key hydroclimatic drivers: SM and VPD across the AGLR from 2000 to 2024. Vegetation dynamics show strong seasonal and interannual variability, closely synchronized with fluctuations in both variables.

Panel (a) of figure 3 highlights the role of SM in sustaining vegetation productivity. Periods of positive SM anomalies are generally associated with elevated NDVI, reflecting favorable growth conditions. In contrast, negative SM anomalies, particularly those exceeding one standard deviation below the mean, coincide with sharp NDVI declines. These patterns are especially pronounced during major drought years such as 2005, 2010, 2016, and 2022, underscoring the critical role of root-zone water availability in supporting photosynthesis across semi-arid and seasonally dry landscapes.

Panel (b) of figure 3 captures the influence of atmospheric dryness. A broadly inverse relationship is observed, whereby high VPD values, signifying dry air and elevated evaporative demand, correspond with negative NDVI anomalies. Conversely, low VPD promotes vegetation growth, especially when combined with adequate soil water availability. Notably, since 2010 the region has experienced an increasing frequency of positive VPD anomalies, pointing to a trend toward heightened atmospheric aridity. This emerging signal suggests that vegetation stress may intensify even in years without severe soil water deficits.

The most severe vegetation declines occur under compound stress events, where negative SM and high VPD coincide. Years such as 2015–2016 and 2022 exemplify this synergy, with concurrent root-zone water depletion and atmospheric dryness producing abrupt and widespread NDVI losses. These compound events represent critical tipping points for vegetation, leading to sharp productivity declines. Nevertheless, rapid NDVI recoveries observed following periods of climatic relief (e.g. post-2008, 2013, and 2019) point to underlying ecosystem resilience, particularly in regions with higher baseline precipitation or vegetation adapted to episodic drought.

Collectively, these results underscore the dual control of vegetation productivity by both soil water availability and atmospheric moisture demand in the AGLR. While SM remains the primary driver of interannual NDVI variability, the growing influence of VPD, potentially driven by regional warming-signals an emerging threat to vegetation resilience under future climate scenarios. These findings emphasize the importance of considering compound hydroclimatic stressors when assessing vegetation vulnerability and forecasting land productivity under climate change.

3.4. Intensification and spatial synchronization of drought events

Figure 4 depicts monthly SPI-3 anomalies across the AGLR from 2000 to 2024, revealing both temporal shifts and an intensifying trend in hydroclimatic extremes. Droughts, classified as moderate ($-1.5 \leqslant \text{SPI} < -1$), severe ($-2 \leqslant \text{SPI} < -1.5$), and extreme ($\text{SPI} < -2$) (table 2), frequently align with key agricultural seasons, particularly the long rains (March–May) and short rains (September–December).

The early 2000 s were characterized by intermittent but impactful drought episodes. Notable events occurred in mid-2004 and mid-2005, with moderate drought conditions affecting the April–July growing period. These episodes correspond with neutral to weakly positive ENSO phases, known to induce rainfall irregularities in the equatorial highlands of East Africa. During this period, the temporal distribution of drought conditions was somewhat isolated, and the affected months rarely extended across successive seasons.

A turning point emerged after 2010. The 2015–2016 El Niño generated one of the most severe and prolonged drought sequences of the past 25 years. Heatmaps reveal successive severe-to-extreme anomalies, peaking in August 2015 and September 2016, disrupting both MAM and OND seasons. This compound failure produced widespread vegetation stress, crop loss, and food insecurity across the region (Nicholson 2017).

Post-2016 droughts became more frequent and spatially synchronized. From 2021 to 2024, moderate-to-severe anomalies recurred almost annually, closely tied to three consecutive La Niña phases (2020–2022). Severe droughts in late 2021 extended into eastern DRC and Burundi, while 2022–2023 events struck during the September–October critical growth window for maize and beans.

The year 2024 exhibits one of the most severe drought signatures of the last two decades, with extreme drought conditions appearing in July, a mid-season month typically associated with peak SM recharge. This event corresponds with a strong El Niño phase coupled with a record-positive IOD, both of which are known to disrupt regional rainfall regimes. The severity and spatial coherence of this event, as captured in the SPI-3 index, reinforce the growing concern over synchronized climate extremes across the region.

Spatial patterns of drought intensity (figure 5) further highlight this transition. Whereas early 2000 s droughts were localized (e.g. July 2002, May–July 2004 in central and eastern DRC), later events became broader and more persistent. December 2005-January 2006 brought extreme anomalies to the Burundian and Rwandan highlands, while the 2015–2017 drought extended across western Tanzania, Burundi, northern Uganda, and Kenya. These events underline the increasing geographical coherence of droughts.

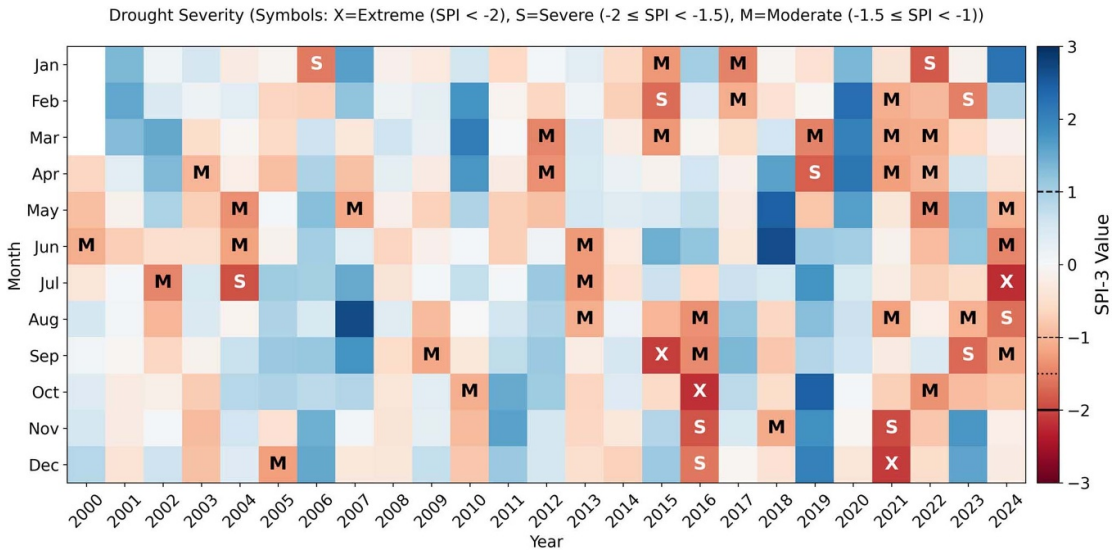

Figure 4. SPI-3 drought analysis by month and year.

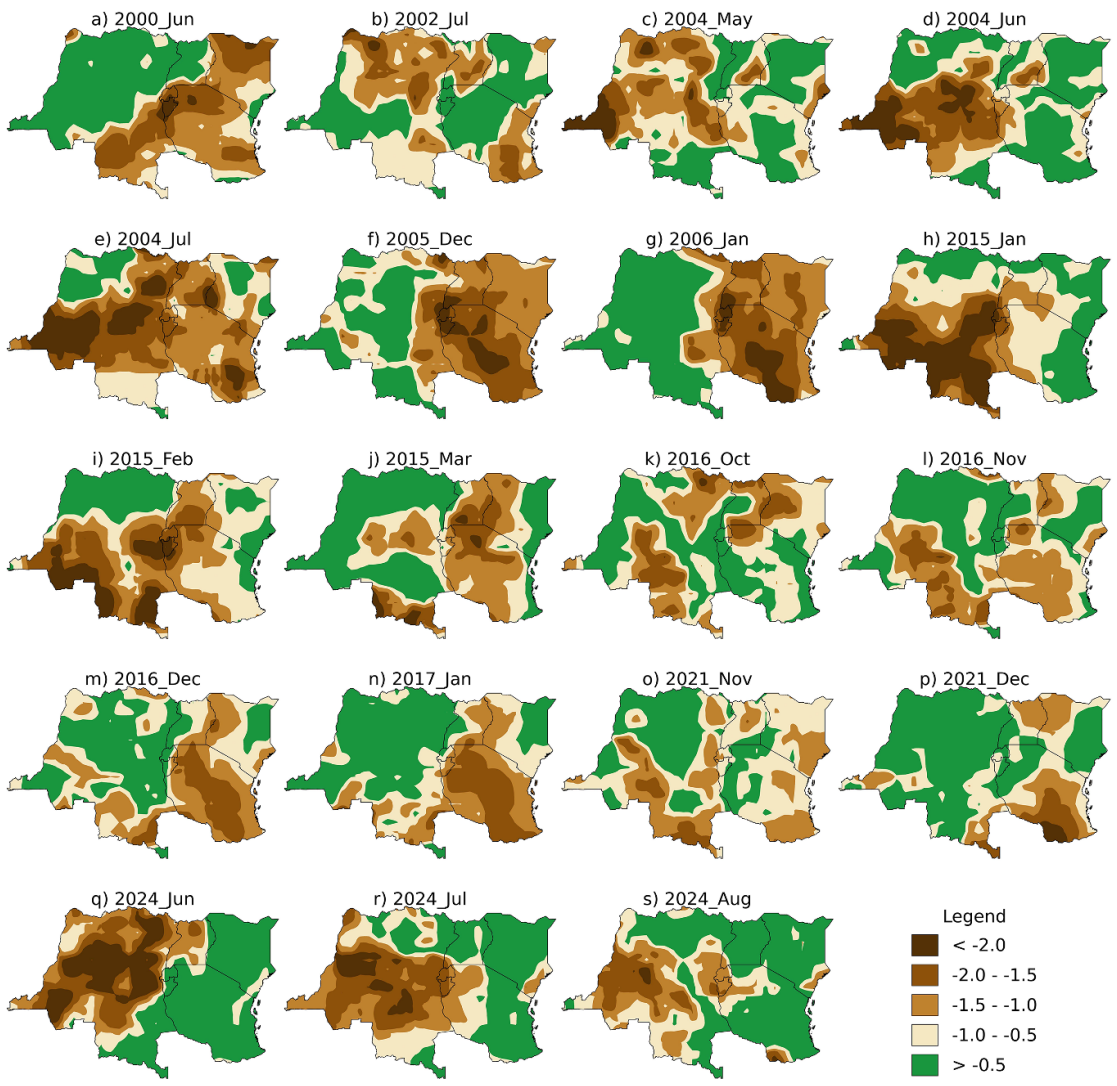

Figure 5. Spatial distributions of drought events and drought intensities based on the 3-month SPI.

Early in the record, droughts were relatively localized, primarily affecting central and eastern DRC. For example, July 2002 and May–July 2004 registered SPI-3 anomalies below −1.5, linked to irregular rainfall during neutral-to-weak ENSO phases. A major intensification followed in December 2005-January 2006, when extreme SPI-3 values (SPI-3 < -2.0) extended into the Burundian and Rwandan highlands and northwestern Tanzania. This episode coincided with failed OND rains and a weak onset of MAM, triggering severe crop failures and water scarcity (Coughlan de Perez *et al* 2019).

A critical shift occurred during the strong 2015–2016 El Niño, which produced one of the longest and most widespread droughts in recent decades. From early 2015 through early 2017, severe-to-extreme anomalies spanned western Tanzania, central DRC, Burundi, and later Kenya, northern Uganda, and southern Rwanda. The persistence of these deficits disrupted both rainy seasons and caused extensive food insecurity across East Africa (Wuestenberg *et al* 2016).

Droughts re-emerged between 2021 and 2024, closely associated with three consecutive La Niña events (2020–2022). These years were marked by suppressed rainfall in both OND and MAM seasons (Anderson *et al* 2023, Funk *et al* 2023). November–December 2021 saw intensification in eastern DRC and Burundi, while the most extreme event occurred in June–August 2024, with SPI-3 < -2 across up to 60% of the region, particularly northwestern Burundi, western Rwanda, and eastern DRC. This latter event coincided with a strong El Niño and a record-positive IOD, producing one of the most synchronized drought signatures in the past quarter century (Funk *et al* 2023).

3.5. Impacts of drought on vegetation greenness and productivity for different land cover types

The AGLR exhibits pronounced intra- and interannual variability in NDVI anomalies across major land cover types-tree cover, shrubland, grassland, and cropland (figure 6). Analysis of standardized NDVI time series from 2000 to 2024, grouped into three eight-year periods, highlights distinct vegetation dynamics shaped by land cover characteristics.

Croplands show the largest seasonal oscillations, with NDVI values ranging from about −1.0 to +1.0, reflecting their acute sensitivity to moisture availability and management practices. Sharp increases occur under favorable growing conditions, while steep declines coincide with droughts or fallow periods, emphasizing the direct influence of SM on agricultural productivity (Ibrahim *et al* 2015, Meng *et al* 2019).

In contrast, areas dominated by tree cover maintain relatively stable NDVI profiles, with fluctuations rarely exceeding ±0.5 standard deviations. This resilience is attributed to deeper rooting systems, higher water storage capacity, and buffering effects against short-term climatic fluctuations (Phiri *et al* 2018, Cui *et al* 2023). Similar trends have been documented in forest ecosystems globally, where perennial vegetation moderates the impacts of climatic and anthropogenic pressures (Eastman *et al* 2013, Meng *et al* 2019).

Interannual NDVI trends (figure 7) show no significant (Mann Kendall test with p-value > 0.05) long-term greening or browning from 2000 to 2024. Across all land cover types, NDVI anomalies fluctuate around the mean, and linear trends remain near zero, indicating that regional vegetation productivity has been broadly maintained despite recurrent climatic extremes and land use pressures. Notable declines appear in grassland and cropland during 2000 and 2021–2022, corresponding to severe droughts that constrained SM and reduced vegetation growth. The latter period aligns with the persistent La Niña conditions that brought reduced rainfall and higher temperatures across the region, underscoring the strong climate sensitivity of herbaceous and cultivated systems compared to tree-dominated covers.

3.6. Seasonal climate-vegetation interactions: The role of ENSO and hydroclimatic drivers

The AGLR's ecosystems are acutely sensitive to seasonal climate variability, yet the interplay between temperature, precipitation, and atmospheric demand, and their combined control on vegetation productivity remains inadequately resolved. To unravel these connections, through a multi-panel visualization (figure 8), we analyze standardized NDVI anomalies against four climatic indicators (temperature T, SPI3, VPD, and SM) across seasons (MAM, SOND, JJA, and DJF), stratified by ENSO phases.

The coupling between atmospheric aridity and soil water availability is further elucidated in the VPD-SM panels (panels (e)–(h) of figure 8). Across all seasons, an inverse relationship is apparent, with years of high VPD generally corresponding to low SM. This coupling is particularly pronounced in MAM and DJF (panels (e) and (h)), where the most severe NDVI deficits are observed when both VPD is elevated and SM is depleted. In contrast, periods with low VPD and high SM tend to support higher NDVI, though the gains above the mean are less dramatic than the losses below it, reflecting an asymmetric, nonlinear vegetation response. The modulation by ENSO phase is evident: El Niño years are disproportionately represented in the high-VPD, low-SM regime, especially during MAM and DJF, while La Niña years more frequently occupy the low-VPD, high-SM space. Nevertheless, the overlap between

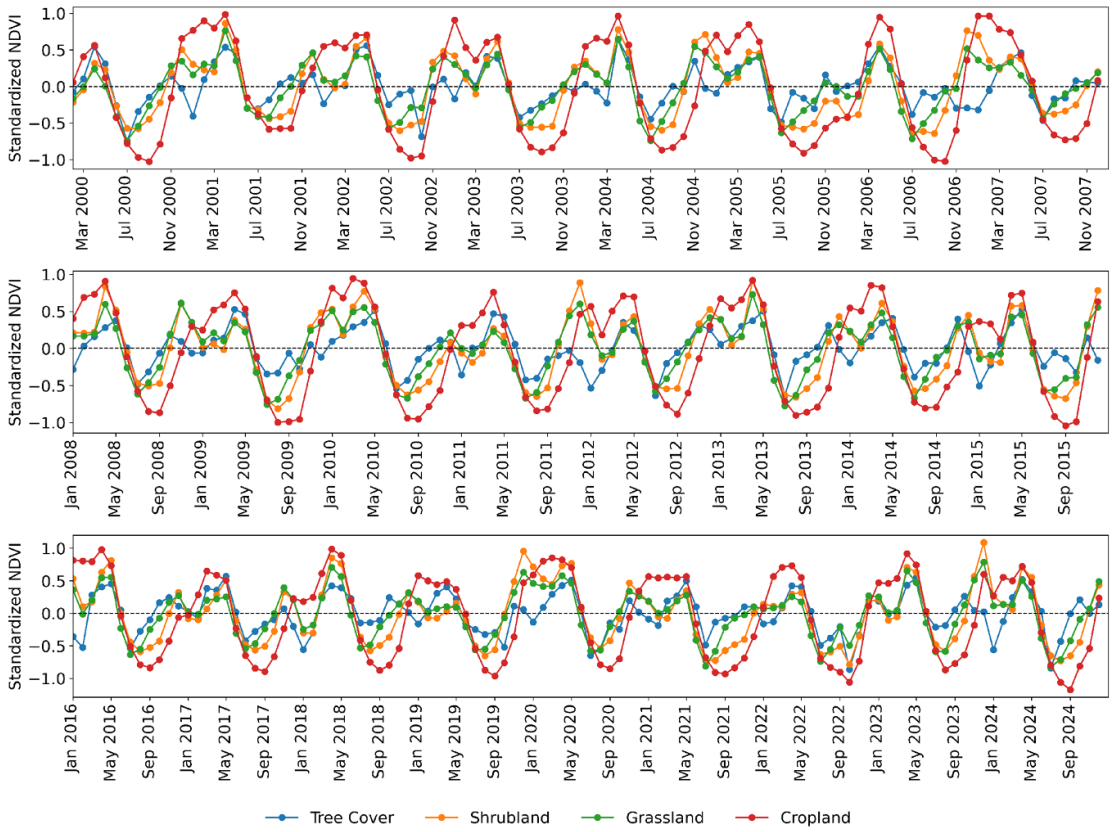

Figure 6. Seasonal NDVI anomalies (2000–2024) for major land cover types in the African Great Lakes region. Time series are presented for cropland, grassland, shrubland, and tree cover.

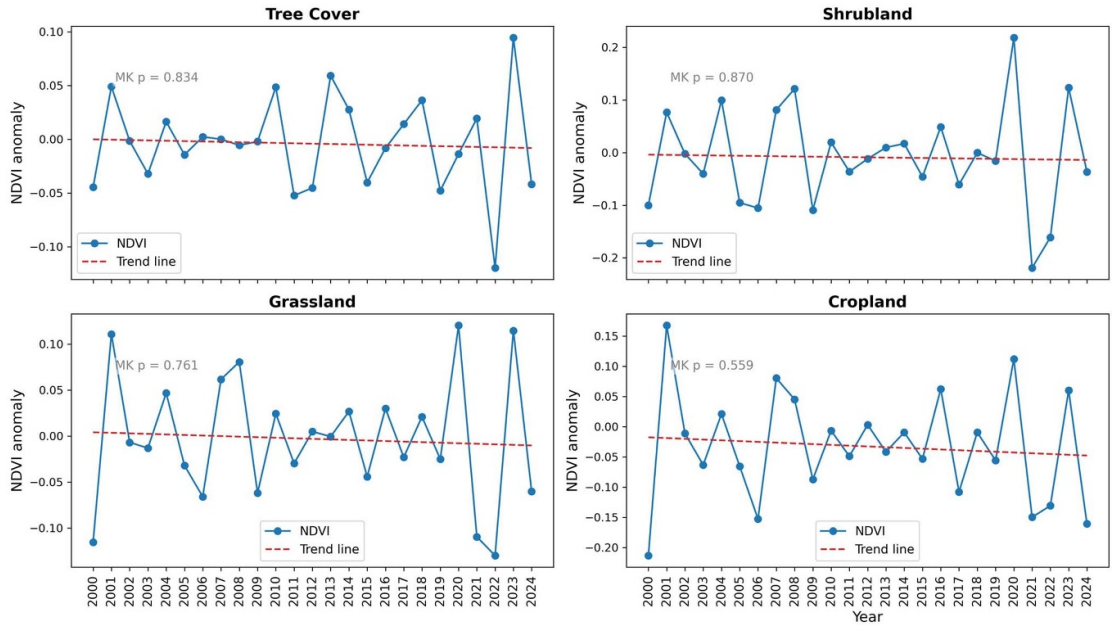

Figure 7. Interannual NDVI anomaly trends by land cover type across the African Great Lakes region (2000–2024). The standardized NDVI time series are shown for cropland, grassland, shrubland, and tree cover.

ENSO phases and NDVI responses suggests that local hydroclimatic interactions, in addition to ENSO, ultimately determine ecosystem outcomes.

A closer inspection of the seasonal panels reveals that MAM (panels (a), (e)) and DJF (panels (d), (h)) are particularly critical periods. In these seasons, the clustering of El Niño years in the hot-dry and

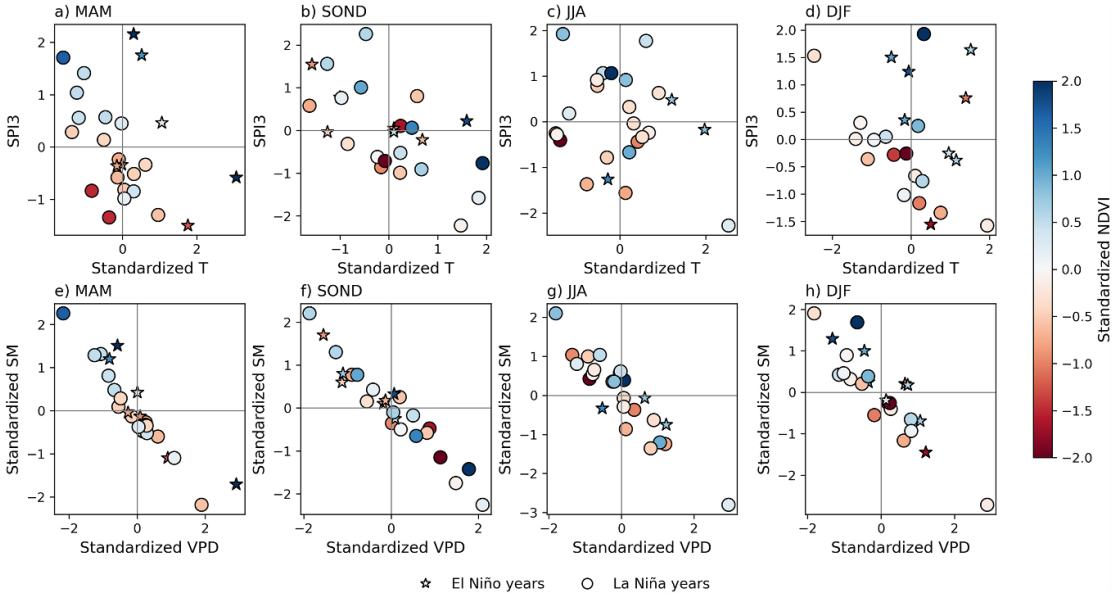

Figure 8. Seasonal climate-vegetation interactions in the African Great Lakes region. Scatterplots of standardized temperature (T) versus SPI3 (a)–(d) and VPD versus soil moisture (SM) (c)–(f) across four seasons (MAM, SOND, JJA, DJF). Marker color denotes standardized NDVI (blue: healthy vegetation, red: stressed), and shapes represent ENSO phases. The plots highlight strong seasonal and interannual variability in climate-vegetation coupling, with El Niño years showing consistently warmer, drier conditions and reduced vegetation greenness. Soil moisture and VPD demonstrate tight coupling and serve as key intermediaries linking climate anomalies to vegetation dynamics.

high-VPD/low-SM quadrants is most pronounced, and the associated NDVI anomalies are at their lowest, indicating acute vegetation stress. The spread of points in these panels also highlights substantial interannual variability, which likely reflects both the direct influence of ENSO and the amplifying effects of local feedbacks between SM and atmospheric demand. In contrast, during SOND and JJA (panels (b), (c), (f), (g)), the separation between ENSO phases is less distinct, and NDVI anomalies are more evenly distributed, suggesting that vegetation in these seasons is less sensitive to ENSO-driven extremes, possibly due to more moderate climatic conditions or differing phenological stages.

These findings illustrate why precipitation-based indices such as SPI3 alone are insufficient predictors of vegetation stress. For instance, in DJF (panel (d)), rainfall deficits alone do not fully account for the observed NDVI reductions; rather, the combined depletion of SM and elevated atmospheric demand explains a much greater fraction of NDVI variability. Integrating both atmospheric demand and soil water supply metrics in drought monitoring and early-warning systems therefore offers a more robust approach for predicting vegetation stress. MAM and DJF emerge as critical leverage points for intervention, as real-time monitoring of VPD and SM, proxies for emergent drought conditions, could provide a 2–3 month lead time for mitigating agricultural losses. As climate change amplifies hydroclimatic extremes, indicators calculated during these periods offer a crucial lens for anticipating ecosystem stress and prioritizing adaptive interventions across this economically vulnerable region.

3.7. Causal discovery of climate-vegetation interactions

Correlation and co-evolution analysis pointed to strong associations between climate variables and vegetation. To move beyond correlation and identify direct causal drivers, we employed the PCMCI algorithm, revealing the complex pathways through which teleconnections and local hydroclimate interact to force vegetation dynamics.

3.7.1. Teleconnections and land-atmosphere feedbacks

Figure 9 depicts a multiscale network linking large-scale teleconnections, regional hydroclimate, and vegetation dynamics. ENSO and DMI emerge as dominant drivers, shaping precipitation, temperature, and vegetation activity, underscoring the key role of ocean-atmosphere interactions in terrestrial ecosystem variability.

At the ocean-atmosphere scale, the ENSO and DMI mutually reinforce one another, with ENSO driving DMI at a 4 month lag and DMI feeding back positively at lags of three to five months. DMI further modulates regional climate by suppressing VPD, increasing SM and P, and lowering T. These

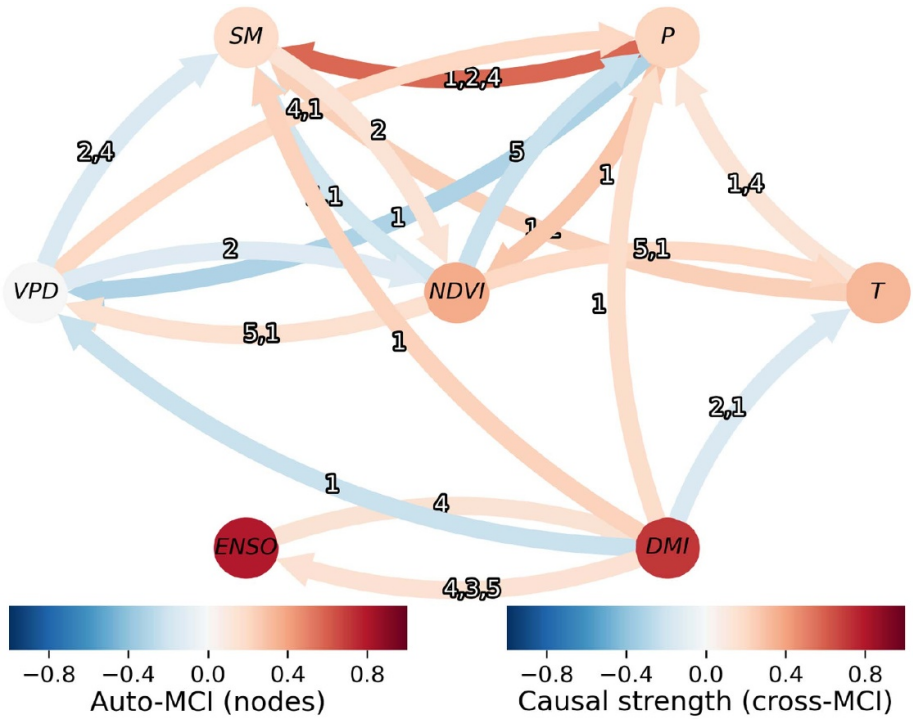

Figure 9. Causal effect analysis of climate factors over NDVI.

pathways highlight the dual role of teleconnections in enhancing water supply while moderating atmospheric demand.

At the regional scale, precipitation and SM form a tightly coupled land-atmosphere feedback. Precipitation also reduces VPD, but its effect on vegetation is lag-dependent: beneficial at short timescales, yet negative at longer lags, consistent with waterlogging or flooding stress. Temperature contributes positively to both precipitation and SM, whereas VPD exerts a drying pressure on soils. Together, these interactions regulate the balance between water supply and evaporative demand.

Vegetation integrates these competing signals while also exerting feedbacks on climate. NDVI responds positively to SM at a two-month lag and precipitation at one-month lag. In turn, vegetation feeds back by enhancing VPD and precipitation while suppressing SM and temperature, underscoring its active role in local hydroclimatic regulation. Collectively, these findings show that vegetation dynamics reflect an emergent compromise between water availability and atmospheric demand, mediated by cascading teleconnections, regional feedbacks, and time-lagged responses that amplify ecosystem vulnerability to climate variability.

3.7.2. Phase-based causal discovery

The phase-based analysis revealed starkly contrasting causal patterns between El Niño and La Niña events (figure 10). During El Niño, the network shows that ENSO anomaly exerts a strong, positive influence on precipitation with a lag of 2–3 months. This increase in precipitation subsequently boosts SM and directly enhances NDVI, the latter with a lag of about 3 months. Precipitation also positively affects NDVI with a lag of 1–3 months, highlighting the critical role of rainfall in driving vegetation greening. VPD is negatively affected by precipitation, indicating that wetter conditions reduce atmospheric demand for water. DMI also interacts with precipitation and NDVI, but its influence is generally weaker compared to ENSO. Temperature appears less central, with faded connections, suggesting its direct role is minor during El Niño in this system.

Conversely, under La Niña conditions, the pattern of interactions changes notably. ENSO anomaly now has a negative (blue) effect on precipitation, SM, and NDVI, with lags ranging from 1 to 5 months. This reflects the typical drying effect of La Niña in the region. Precipitation remains a central driver of NDVI, but the overall direction of influence is negative, indicating suppressed vegetation growth. The feedbacks between variables such as VPD, SM, and NDVI remain, but the pathways are more complex,

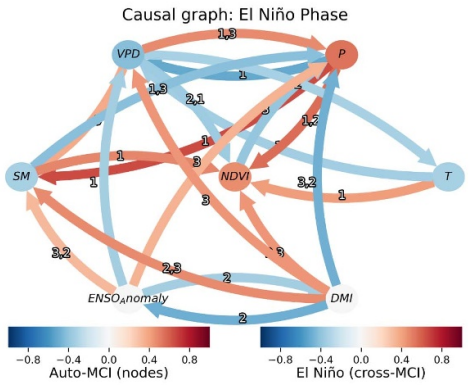

(a) El Niño phase: ENSO strengthens rainfall, which cascades through soil moisture to enhance NDVI, while reducing VPD-driven stress.

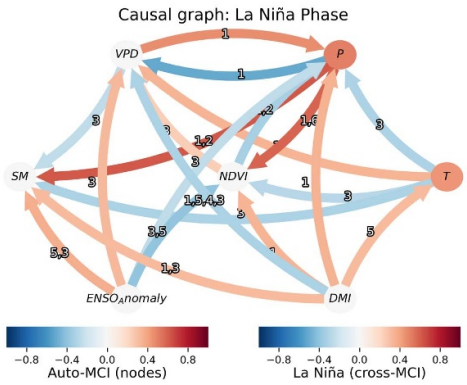

(b) La Niña phase: ENSO suppresses rainfall and soil water, amplifying vegetation stress via VPD and weakening NDVI.

Figure 10. ENSO-phase causal networks of climate-vegetation interactions in the African Great Lakes region. Arrow thickness denotes effect strength; numbers represent time lags (months).

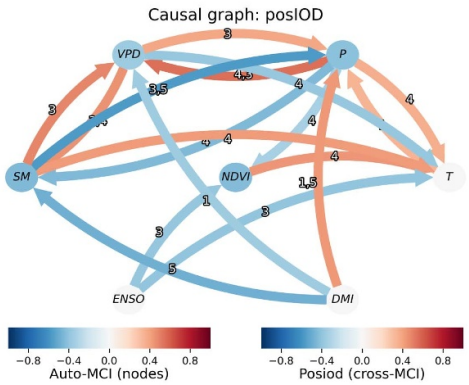

(a) Positive IOD: DMI drives NDVI both directly and indirectly through soil moisture and VPD, highlighting compounded stress pathways.

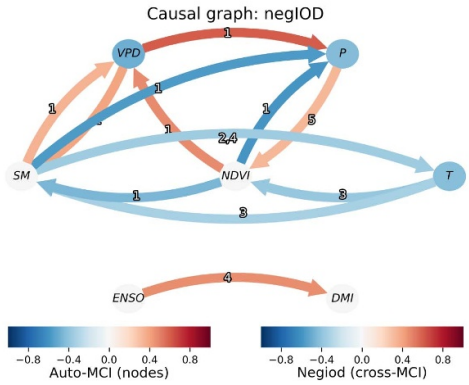

(b) Negative IOD: Causal links weaken, ENSO–DMI coupling reappears, and NDVI centrality diminishes.

Figure 11. IOD-phase causal networks in the African Great Lakes region. Arrow colors indicate positive (red) or negative (blue) effects; thickness scales with effect strength.

with multiple lagged effects and generally weaker positive feedbacks. DMI and temperature play more visible roles, with temperature exerting a positive influence on NDVI and precipitation, especially at longer lags.

Similarly, the causal influence of the IOD is phase-dependent, with strong, coherent pathways during positive IOD events and a sparser, weaker network during negative IOD phases (figure 11). During positive IOD (IOD+) conditions, DMI was identified as a central causal driver, with strong and direct causal influences on NDVI, VPD, and temperature. Multiple converging causal pathways toward SM were also evident, suggesting that IOD+ affects vegetation both directly (via NDVI) and indirectly through compounded thermal and hydric stress. NDVI was the most centrally connected node in the network, indicating its sensitivity to climatic perturbations during IOD+ periods.

Conversely, under negative IOD (IOD−) conditions, the causal network was sparser and the magnitudes of causal links were weaker. The DMI still influenced NDVI, temperature, and VPD, but with less intensity and coherence. The ENSO-to-DMI causal path re-emerged during this phase, implying a greater role of background ENSO variability in shaping IOD dynamics when DMI is negative. The centrality of NDVI within the causal graph was reduced, indicating a lower level of coordination between vegetation dynamics and hydroclimatic variables under IOD−.

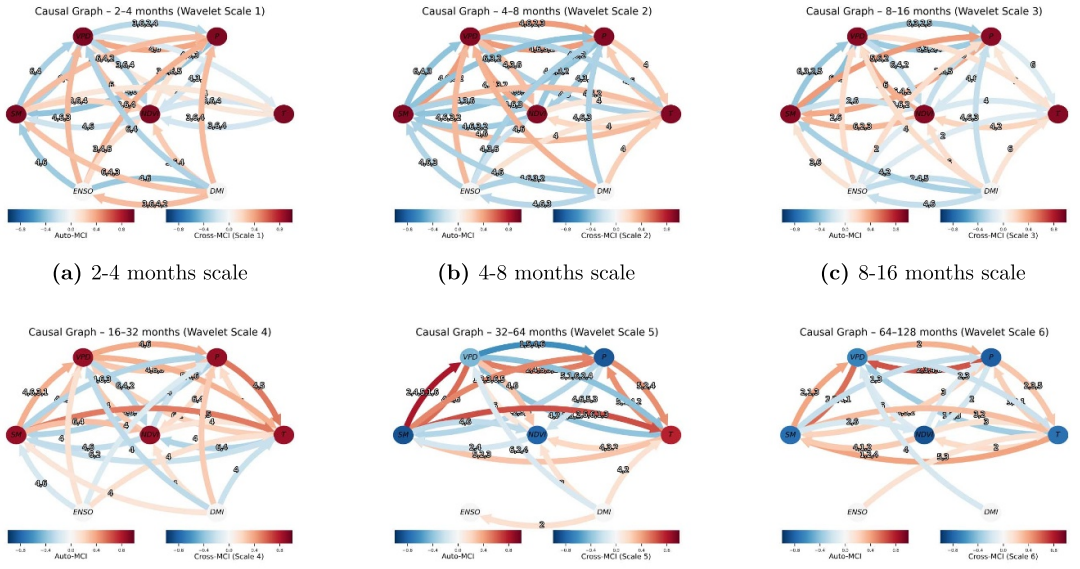

(a) 2-4 months scale (b) 4-8 months scale (c) 8-16 months scale

(d) 16-32 months scale (e) 32-64 months scale (f) 64-128 months scale

Figure 12. Scale-dependent causal networks of climate-vegetation interactions revealed by wavelet decomposition. Panels (a)–(f) show causal graphs across sub-seasonal (2–4 months) to decadal (64–128 months) scales. Arrows denote direction, color represents sign (red = positive, blue = negative), and numbers indicate lag in months.

3.7.3. Multiscale causal discovery

The wavelet-based analysis (figure 12) revealed a clear hierarchy of drivers across temporal scales. At sub-seasonal scales (2–4 months, figure 12(a)), VPD consistently emerged as the primary direct driver of NDVI, with rapid effects (2 month lags). Causal analysis identifies robust pathways with lags of 2–6 months, indicating that increases in VPD induce rapid hydraulic stress, leading to NDVI suppression within as little as two months. The persistence of these effects for up to six months suggests extended impacts on SM and root-zone water availability.

Simultaneously, SM demonstrates bidirectional coupling with NDVI. Negative lags indicate that prior vegetation states influence SM through transpiration and canopy shading, while positive lags show that SM deficits precede NDVI declines by approximately two months. NDVI also shows strong autoregressive persistence (Auto-MCI), but this intrinsic stability is frequently disrupted by external climate forcing, particularly by VPD. In contrast, the DMI exhibits only weak, symmetric causal weights, suggesting minimal direct influence at this timescale.

At seasonal scales (4–8 month, figure 12(b)), VPD remains a dominant driver, with both immediate (2–3 months) and delayed (6–7 months) effects on NDVI. Precipitation acts as a dual-phase modulator: short lags (2–3 months) correspond to rapid greening, while longer lags (4–6 months) reflect delayed impacts on subsurface water reserves. Large-scale climate modes, including ENSO and DMI, exert structured, direct influence on NDVI through consistent lag pathways (4, 6, 3 months), primarily by modulating regional VPD and precipitation regimes.

At the 8–16 month scale, ENSO and DMI become the primary orchestrators of ecosystem dynamics. Their synchronized lag patterns reveal a teleconnected cascade: ENSO reorganizes Pacific moisture fluxes, which realign DMI within four months, subsequently amplifying VPD and depleting SM within six months, ultimately suppressing NDVI after three months. SM acts as a pivotal relay, translating macroclimate signals into ecosystem impacts. Bidirectional feedbacks, evident in symmetric Cross-MCI weights, confirm that vegetation actively modulates soil water via evapotranspiration, establishing climate-vegetation memory at this scale.

In contrast to the rapid, direct influence of VPD at shorter scales, the analysis reveals that large-scale teleconnections like ENSO and IOD exert their strongest influence at interannual and decadal scales (figures 12(d)–(f)). Their effects are not direct but are mediated through slower, indirect pathways that modulate regional hydroclimatic variables. Within this hierarchy, SM consolidates its role as the dominant mediator, integrating these long-term climate signals.

A clear causal progression emerges: ENSO teleconnections progressively drain deep soil reservoirs over approximately six months, which culminates in an NDVI response after about three months. VPD, meanwhile, continues to exert rapid stress during extreme events at a 1 month lag. This dynamic creates

cross-scale feedback; for instance, NDVI deficits from prior droughts can reduce SM retention, fostering self-reinforcing dry spells.

At the 32–64 month scale, interactions become more complex and threshold-driven. The influence of VPD extends over 5–6 month lags, reflecting longer-term ecosystem impacts such as carbon starvation and canopy loss. Precipitation exhibits a bimodal effect: convective rains impact vegetation within two months, while their contribution to groundwater recharge influences ecosystem resilience at seven months. The direct causal role of ENSO diminishes here, suggesting a saturation of its teleconnection efficiency at these scales.

Finally, at decadal scales (64–128 months), legacy effects and ecosystem memory dominate. While VPD remains relevant for immediate stress on a 1–3 year scale, ultra-long lags between SM and NDVI (12–48 months) suggest slower ecosystem restructuring, such as species turnover, shifts in root architecture, or soil carbon loss. Oceanic modes show no direct, structured causality, confirming their impacts are fully mediated and integrated through shorter-scale processes. At this decadal level, vegetation dynamics appear governed more by these internal ecosystem state transitions than by direct atmospheric forcing.

3.8. Discussion

3.8.1. Compound climate drivers of vegetation stress

Our findings reveal that vegetation decline in the AGLR is predominantly driven by compound drought stress, characterized by the co-occurrence of low SM and high VPD. The most severe negative NDVI anomalies consistently coincide with these compound conditions (figures 5, 2), indicating that extreme vegetation stress in the region is largely associated with combined soil and atmospheric aridity rather than with single-factor anomalies. This finding supports a growing body of physiological and observational evidence on the disproportionate impacts of hot droughts, during which elevated VPD forces stomatal closure and suppresses carbon assimilation even before critical soil water depletion occurs (Grossiord *et al* 2020). Recent regional assessments further indicate that high atmospheric dryness can amplify drought impacts by 30%–50% beyond the effects of precipitation deficits alone (Babaousmail *et al* 2024, Zeraati *et al* 2024).

This study builds upon earlier work identifying SM drought as a central driver of agricultural and ecological impacts in East Africa (Liu *et al* 2022, Xu *et al* 2024), while advancing understanding by explicitly resolving causal pathways. The applied PCMCI framework reveals that SM depletion alone is often insufficient to explain severe vegetation decline. Instead, compound SM-VPD stress emerges as the predominant direct driver, highlighting the importance of land-atmosphere coupling in regulating vegetation responses. By moving beyond pattern-based attribution, our analysis traces this compound stress upstream to large-scale climate drivers. In particular, warming of the Indian Ocean and associated intensification of the Walker circulation (Funk *et al* 2023) modulate the regional co-occurrence of SM deficits and elevated VPD. Concurrently, SM depletion is reinforced not only by seasonal rainfall deficits but also by changes in intraseasonal rainfall structure, including a shortening of the wet season and lengthening of dry spells (Wainwright *et al* 2019, Palmer *et al* 2023). The interaction of circulation-driven atmospheric drying and rainfall-distribution-driven SM loss, often phase-locked to El Niño and positive IOD events, produces the nonlinear vegetation impacts characteristic of hot droughts.

Major El Niño events, particularly during 2015–2016, exemplify this mechanism, having triggered widespread NDVI declines and gross primary productivity losses of approximately 18%–25% across tropical ecosystems (Liu *et al* 2017, Xu *et al* 2024), with pronounced consequences for regional agriculture and food security (Qu *et al* 2019). Over the past 25 years, such compound droughts have intensified and become increasingly spatially synchronized, a shift that has been especially evident since 2010 within the Burundi–Rwanda-northwestern Tanzania corridor. This emerging hotspot is linked to altered Intertropical Convergence Zone dynamics, strengthened land-atmosphere feedbacks (Haile *et al* 2020), and modulation by Atlantic Niño variability (Tall *et al* 2023). Local processes, including moisture recycling from Lake Victoria and orographic controls, further modulate these large-scale signals, generating spatial heterogeneity, for example, the contrasting rainfall conditions observed between southwestern Uganda and eastern DRC during late 2016-early 2017.

The Burundi–Rwanda–Tanzania corridor emerges as a region of persistent vulnerability, experiencing repeated compound drought events since 2015. Given the dominance of rain-fed agricultural and pastoral systems, vegetation in this subregion exhibits prolonged recovery times following major compound stress events, consistent with documented legacy effects on ecosystem carbon stocks and vegetation structure (Wigneron *et al* 2020). These findings underscore that the impacts of compound droughts

extend beyond immediate productivity losses, imposing longer-term constraints on ecosystem resilience. Addressing this growing risk requires strengthening regional early-warning and nowcasting systems that explicitly integrate compound indicators such as VPD-SM interactions, alongside the promotion of climate-resilient agricultural practices designed to buffer both atmospheric and SM stress (AghaKouchak *et al* 2015, Dorigo *et al* 2017).

3.8.2. Operational and policy implications

Our demonstration that integrated VPD-SM metrics provide 2–3 month lead times for NDVI-based stress detection represents a potentially transformative shift in drought monitoring. Current operational indices, such as the SPI, often fail to capture vegetation responses in heterogeneous and fragmented landscapes. Zita *et al* (2025) showed that SPI explains less than 40% of NDVI variability in East Africa, whereas VPD-SM models account for more than 70%. The operational relevance of these findings is already evident: the IGAD climate prediction and applications centre reported a 22% reduction in agricultural losses in Kenya in 2023 following the deployment of VPD-informed drought advisories. These results underscore the potential of coupling remote sensing with ecophysiological indicators to strengthen early warning systems.

Enhancing ecosystem resilience in the AGLR will require protecting intact forests, which play a crucial role in sustaining regional moisture cycling. In parallel, deploying low-cost VPD sensors in smallholder systems could support more adaptive irrigation practices. Emerging smart irrigation systems piloted in Tanzania, for instance, have already reduced yield losses by 15%–30% under elevated VPD conditions (Anderson *et al* 2023).

3.8.3. Land cover modulation and ecosystem buffering

The resilience of ecosystems to climatic stressors is profoundly influenced not just by climate variables, but also by land cover structure and type. The distribution of tree cover in the AGLR exemplifies this, demonstrating significantly greater stability in NDVI values, typically varying within ± 0.5 standard deviations. In contrast, croplands and shrublands exhibit fluctuations that can extend up to ± 1.0 standard deviations, emphasizing the role of ecosystem structure in mediating resilience to climatic extremes. Research indicates that tree-covered areas, particularly forests with dense canopies, effectively regulate microclimatic conditions, sustaining transpiration-driven humidity and consequently suppressing local VPD levels (Hardwick *et al* 2015, Staal *et al* 2018, Cui *et al* 2023)

The higher instability observed in cropland ecosystems underscores their sensitivity to environmental fluctuations, primarily due to shallow root systems and diminished evapotranspiration levels, especially in monoculture agricultural settings (Abel and Samuel 2024) In the AGLR, the situation is exacerbated by agricultural fragmentation, which leads to a moisture recycling capacity reported to be significantly lower in smallholder-dominated landscapes compared to intact forest ecosystems, thus undermining their potential to buffer atmospheric stresses. Kayiranga *et al* (2022) estimated that smallholder-dominated landscapes have moisture recycling capacities 15%–40% lower than those of intact forest ecosystems, reducing their ability to buffer against atmospheric stress. Shrublands, which often dominate degraded lands, are even more sensitive. Their high NDVI variability may reflect strong fire-climate feedbacks, where drought-induced fuel dryness increases burn severity and suppresses regrowth, as observed by Anderson *et al* (2023). Notably, the post-2015 period has seen a 25% increase in VPD anomalies in the region, a trend mirrored in the broader African context where declining relative humidity is driving VPD increases at twice the rate of warming (Humphrey *et al* 2021). These findings reinforce the notion that fragmented, low-biomass landscapes are disproportionately vulnerable to the emerging regime of atmospheric aridity.

3.8.4. Vegetation recovery and ecosystem memory

Our analysis highlights a notable asymmetry in vegetation recovery following major hydroclimatic events. NDVI tends to rebound relatively quickly-within three to six months-following La Niña episodes. In contrast, recovery after El Niño-induced declines can take nine to twelve months, revealing the presence of ecosystem memory and legacy effects. This hysteresis suggests that AGLR ecosystems exhibit memory effects-likely due to hydraulic damage, loss of canopy biomass, and degradation of root systems. Wigneron *et al* (2020) found similar legacy effects in African forests, where carbon fluxes did not return to pre-event levels even two years after the 2015–2016 El Niño.

In croplands, recovery delays may be further exacerbated by loss of soil organic matter and reduced water-holding capacity, especially under repeated droughts. Raghuraman *et al* (2024) demonstrated that in AGLR maize systems, crop losses following consecutive droughts (e.g. 2016 and 2020) rose from 20% to 45%, illustrating how compounding events erode ecosystem recovery. This pattern is not confined to

Africa: Bastos *et al* (2020) observed similar multiyear 'carbon debts' in European ecosystems following back-to-back heatwaves and droughts. In the AGLR, the 40% increase in high-VPD months since 2015 is likely accelerating these legacy effects, placing ecosystems in a dangerous feedback loop where repeated stressors suppress recovery. This evolving dynamic is consistent with SSP3-7.0 scenarios, which project intensifying drought conditions and rising VPD across East Africa (Lee *et al* 2023).

3.8.5. Emerging atmospheric aridity and predictive indicators

The post-2015 surge in VPD anomalies thus marks more than a climatic anomaly, it reflects a broader atmospheric transition with profound ecological consequences. Our analysis aligns with the work of Funk *et al* (2023), who identified Indian Ocean warming as the primary driver of rising VPD across East Africa, via enhanced moisture divergence from land surfaces. This 'drying atmosphere' effect undermines ecosystem water-use efficiency (WUE), even under conditions of near-normal rainfall. Across the continent, Zhang *et al* (2024) reported 5%–10% declines in WUE since 2000, closely linked to VPD increases. In the AGLR, this trend is already impacting rainfed agriculture: field surveys conducted between 2020 and 2024 in Uganda and Kenya indicate that irrigation requirements rose by 30% compared to the 2000–2014 period, despite no significant decrease in rainfall. These results highlight the inadequacy of precipitation-based monitoring tools for anticipating vegetation stress. Crucially, VPD anomalies often precede observable SM depletion by several weeks, offering a predictive window that rainfall metrics alone cannot capture. This temporal lead, also observed in Sahelian systems, positions VPD as a key target for anticipatory adaptation.

3.8.6. Research gaps and future directions

This study characterizes the dominant climate–vegetation dynamics at the regional scale of the AGLR. The analysis of aggregated time series reveals large-scale climatic mechanisms, while the broad land-cover stratification demonstrates differential ecosystem sensitivities. A key consideration is that localized factors, particularly anthropogenic irrigation, can modify relationships at the field scale. However, due to its limited spatial extent, irrigation's signal is subordinate in our aggregated results. Our findings are thus most applicable to understanding the vulnerability of the region's predominant rain-fed systems.

Several methodological considerations provide context for our findings and outline clear research frontiers. The PCMCI framework advances beyond correlation, yet its inferred networks represent statistically dominant time-asymmetric dependencies rather than definitive mechanistic proofs. In a coupled system, links (e.g. SM $\rightarrow$ NDVI) likely capture the net signal of bidirectional feedbacks operating at sub-monthly scales. Furthermore, while we included major teleconnections, the principle of causa proxima applies, and unobserved common drivers could confound some links. The analysis also assumes stationarity within each classified climate phase, which may obscure evolving relationships during long events.

Building on this work, specific future directions emerge. First, our multiscale analysis isolates drivers at distinct frequencies but does not quantify interactions across scales-such as how interannual ENSO variability modulates seasonal VPD-NDVI coupling. Methodologies like wavelet coherence or scale-recursive PCMCI could reveal this hierarchical structure. Second, while two decades of MODIS data capture meaningful trends, higher-resolution imagery (e.g. Sentinel-2) is needed to resolve fine-scale heterogeneity in smallholder landscapes (Ayugi *et al* 2022). Third, future studies should integrate causal discovery with physically based land surface models to disentangle bidirectional mechanisms and explicitly quantify land-use feedbacks (e.g. irrigation's buffering role). Fourth, integrating paleoclimatic archives (Nicholson 2017) could contextualize recent aridity trends within longer-term variability. Finally, downscaling CMIP6 projections to evaluate NDVI responses under scenarios like SSP2-4.5 and SSP5-8.5 will be vital for guiding long-term, scenario-based adaptation planning in the AGLR.

4. Conclusion

This study provides a comprehensive, multiscale assessment of how climatic variability shapes vegetation productivity in the AGLR. By combining MODWT wavelet decomposition with PCMCI causal discovery, we identified both the immediate and delayed influences of key hydroclimatic variables; precipitation, SM, VPD, and large-scale climate modes (ENSO, IOD), on vegetation greenness (NDVI). Our findings highlight that vegetation stress is rarely driven by single factors. Instead, compound conditions of high VPD and low SM emerge as the predominant direct driver of severe vegetation decline, particularly during El Niño years, underscoring the necessity of integrated climate monitoring approaches.

The results also reveal strong land cover-dependent sensitivities. Croplands and shrublands exhibit large NDVI variability and prolonged recovery times after droughts, whereas tree-covered areas display

greater resilience due to their capacity to buffer microclimatic extremes and maintain water availability. Causal analysis across temporal scales shows that VPD dominates at sub-seasonal to seasonal scales, while ENSO and IOD exert stronger influence at interannual and decadal scales. Notably, post-2015 data indicate an intensifying atmospheric aridity trend, with a pronounced increase in high-VPD months compared to the early 2000s, suggesting emerging risks for agricultural and ecological stability.

Operationally, the demonstrated 2–3 month predictive lead time of compound VPD-SM metrics for vegetation stress provides a clear rationale for their integration into operational regional drought early-warning systems. This specific finding translates to actionable measures, such as issuing VPD-based agricultural advisories before the critical growing season and prioritizing reservoir water allocation based on rising atmospheric aridity forecasts. Furthermore, the marked stability of intact forest ecosystems under compound stress, evidenced by our land-cover analysis, provides a data-driven argument for prioritizing forest protection in agricultural landscapes as a targeted, ecosystem-based adaptation strategy to mitigate local VPD increases.

Looking forward, our approach offers a framework for climate-vegetation analysis that can be replicated across other climate-sensitive regions. Future work should integrate Sentinel-class imagery to resolve fine-scale heterogeneity, use paleoclimate archives to contextualize recent aridity trends, and employ downscaled CMIP6 projections to explore vegetation responses under plausible future climate scenarios. By advancing from climate correlation to climate causation, this study strengthens the foundation for anticipatory adaptation strategies that can safeguard both ecosystems and livelihoods in the AGLR and beyond.

Acknowledgments

The authors gratefully acknowledges the financial support of the Académie de Recherche et de l'Enseignement Supérieur (ARES) through a Postdoctoral Research Fellowship awarded to P B. We sincerely thank the institutions that provided the foundational data for this study. The European Centre for Medium-Range Weather Forecasts (ECMWF) and the U.S. Geological Survey (USGS) Climate Hazards Center produced the ERA5-Land and CHIRPS datasets, respectively. The National Aeronautics and Space Administration (NASA) provided the MODIS vegetation products. Climate indices were sourced from the National Oceanic and Atmospheric Administration (NOAA)

Data availability statement

The data supporting the findings of this study are derived from publicly available datasets (ERA5-Land, CHIRPS, MODIS, NCEP NOAA, and PSL NOAA), all of which are cited in the references section. ENSO data can be found at https://origin.cpc.ncep.noaa.gov/products/analysis_monitoring/ensostuff/ONI_v5.php. DMI is available at https://psl.noaa.gov/gcos_wgsp/Timeseries/Data/dmi.had.long.data.

The data that support the findings of this study will be openly available after acceptance (but before publication) at the following URL/DOI:. https://github.com/Pacifique-BATUNGWANAYO/Multiscale-Causal-Analysis (Batungwanayo 2026). Data will be available from 4 September 2026.

Supplementary data 1 available at https://doi.org/10.1088/2752-5295/ae4cc1/data1.

Funding

This study was supported by the Académie de Recherche et de l'Enseignement Supérieur (ARES)

Conflict of interest

The authors declare no competing financial or other conflicts of interest.

Author contributions

Pacifique Batungwanayo 0000-0003-1748-7604
Conceptualization (lead), Data curation (lead), Formal analysis (lead), Methodology (lead), Resources (lead), Software (lead), Validation (lead), Visualization (lead), Writing – original draft (lead), Writing – review & editing (equal)

Marnik Vanclooster 0000-0003-1358-8723
Conceptualization (supporting), Funding acquisition (lead), Investigation (lead), Methodology (equal), Project administration (lead), Supervision (lead), Writing – review & editing (equal)

Athanase Nkunzimana 0000-0003-1675-1522
Formal analysis (supporting), Investigation (supporting), Methodology (supporting), Validation (supporting), Writing – review & editing (supporting)

References

Abel O and Samuel A 2024 Gis-based characterization of land use, land cover patterns and microclimate of agricultural and agroforestry landscapes in a rainforest zone of nigeria *Int. J. Environ. Clim. Change* **14** 1002–23

AghaKouchak A, Farahmand A, Melton F S, Teixeira J, Anderson M C, Wardlow B D and Hain C R 2015 Remote sensing of drought: progress, challenges and opportunities *Rev. Geophys.* **53** 452–80

Anderson W, Cook B I, Slinski K, Schwarzwald K, McNally A and Funk C 2023 Multiyear la niña events and multiseason drought in the horn of africa *J. Hydrometeorol.* **24** 119–31

Anyamba A, Glennie E and Small J 2018 Teleconnections and interannual transitions as observed in african vegetation: 2015–2017 *Remote Sens.* **10** 1038

Assis P H d S, Luz J M, Gallis R B d A, Maciel G M, Oliveira R C d, Borges R T d O and Siquieroli A C 2024 Vegetation indices for monitoring agronomic performance of potato under combinations of mineral and organic fertilization *Rev. Bras. Eng. Agri. Amb.* **28** e278100

Ayugi B *et al* 2022 Review of meteorological drought in africa: historical trends, impacts, mitigation measures and prospects *Pure Appl. Geophys.* **179** 1365–86

Babaousmail H, Ayugi B O, Hammad Z, Alupot D, Posset K R, Mumo R and Rajasekar A 2024 Quantifying drought impacts based on the reliability–resiliency–vulnerability framework over East Africa *Climate* **12** 92

Bamston A G, Chelliah M and Goldenberg S B 1997 Documentation of a highly enso-related SST region in the equatorial pacific: research note *Atmos.-Ocean* **35** 367–83

Bastos A *et al* 2020 Direct and seasonal legacy effects of the 2018 heat wave and drought on european ecosystem productivity *Sci. Adv.* **6** eaba2724

Batungwanayo P 2026 Multiscale causal analysis dataset and code for vegetation decline in the African Great Lakes region *GitHub repository: Multiscale-Causal-Analysis* (available at: https://github.com/Pacifique-BATUNGWANAYO/Multiscale-Causal-Analysis)

Batungwanayo P, Vanclooster M, Alonso A and Frendy Koropitan A 2024 Wavelet-based analysis of hydro-climatic and vegetation dynamics in heterogeneous agro-climatic zones of east africa *J. Water Clim. Change* **15** 4054–75

Bevacqua E, Suarez-Gutierrez L, Jézéquel A, Lehner F, Vrac M, Yiou P and Zscheischler J 2023 Advancing research on compound weather and climate events via large ensemble model simulations *Nat. Commun.* **14** 2145

Blau M and Ha K-J 2020 The Indian Ocean Dipole and its impact on east african short rains in two cmip5 historical scenarios with and without anthropogenic influence *J. Geophys. Res.: Atmos.* **125** e2020JD033121

Cook B I, Anderson W, Slinski K, Shukla S and McNally A 2024 Investigating the strength and variability of el niño–Southern Oscillation teleconnections to hydroclimate and maize yields in Southern and East Africa *J. Hydrometeorol.* **25** 257–75

Cordeiro M C, Martinez J-M and Peña-Luque S 2021 Automatic water detection from multidimensional hierarchical clustering for sentinel-2 images and a comparison with level 2a processors *Remote Sens. Environ.* **253** 112209

Coughlan de Perez E, van Aalst M, Choularton R, van den Hurk B, Mason S, Nissan H and Schwager S 2019 From rain to famine: assessing the utility of rainfall observations and seasonal forecasts to anticipate food insecurity in East Africa *Food Secur.* **11** 57–68

Cui M, Zheng X, Li Y and Wang Y 2023 Analysis of ndvi trends and driving factors in the buffer zone of the aral sea *Water* **15** 2473

De Keersmaecker W, Lhermitte S, Tits L, Honnay O, Somers B and Coppin P 2015 A model quantifying global vegetation resistance and resilience to short-term climate anomalies and their relationship with vegetation cover *Glob. Ecol. Biogeogr.* **24** 539–48

Didan K 2021 MODIS/Aqua vegetation indices 16-Day L3 global 250m SIN grid V061 *NASA EOSDIS Land Processes Distributed Active Archive Center (DAAC) Data Set* (https://doi.org/10.5067/MODIS/MYD13Q1.061)

Ding Y, Feng Y, Chen K and Zhang X 2024 Analysis of spatial and temporal changes in vegetation cover and its drivers in the aksu river basin, China *Sci. Rep.* **14** 10165

Dorigo W *et al* 2017 ESA CCI soil moisture for improved earth system understanding: state-of-the art and future directions *Remote Sens. Environ.* **203** 185–215

Du S, Wang M, Wei N, Mwachala G, Hu G, Wu L, Wang S and Wang Q 2023 Contributions to the flora of tropical East Africa *Plants* **12** 1336

Dunning C M, Black E C and Allan R P 2016 The onset and cessation of seasonal rainfall over Africa *J. Geophys. Res.: Atmos.* **121** 11–405

Eastman J R, Sangermano F, Machado E A, Rogan J and Anyamba A 2013 Global trends in seasonality of normalized difference vegetation index (NDVI), 1982–2011 *Remote Sens.* **5** 4799–818

FAO 2022 *The state of food security and nutrition in the world 2022: repurposing food and agricultural policies to make healthy diets more affordable 2022* Food and Agriculture Org (https://doi.org/10.4060/cc0639en)

Fer I, Tietjen B, Jeltsch F and Wolff C 2017 The influence of el niño–Southern Oscillation regimes on eastern african vegetation and its future implications under the rcp8. 5 warming scenario *Biogeosciences* **14** 4355–74

Funk C *et al* 2015 The climate hazards infrared precipitation with stations-a new environmental record for monitoring extremes *Sci. Data* **2** 1–21

Funk C, Fink A H, Harrison L, Segele Z, Endris H S, Galu G, Korecha D and Nicholson S 2023 Frequent but predictable droughts in east africa driven by a walker circulation intensification *Earth's Future* **11** e2022EF003454

Grossiord C, Buckley T N, Cernusak L A, Novick K A, Poulter B, Siegwolf R T, Sperry J S and McDowell N G 2020 Plant responses to rising vapor pressure deficit *New Phytol.* **226** 1550–66

Haile G G, Tang Q, Hosseini-Moghari S-M, Liu X, Gebremicael T, Leng G, Kebede A, Xu X and Yun X 2020 Projected impacts of climate change on drought patterns over East Africa *Earth's Future* **8** e2020EF001502

Haile G G, Tang Q, Sun S, Huang Z, Zhang X and Liu X 2019 Droughts in east africa: causes, impacts and resilience *Earth-Sci. Rev.* **193** 146–61

Hardwick S R, Toumi R, Pfeifer M, Turner E C, Nilus R and Ewers R M 2015 The relationship between leaf area index and microclimate in tropical forest and oil palm plantation: forest disturbance drives changes in microclimate *Agric. Forest Meteorol.* **201** 187–95

Hodgkins R, To L S and Matthews T 2025 The ipcc reports and he geography: opportunities lost and found *J. Geogr. Higher Educ.* **49** 141–53

Humphrey V, Berg A, Ciais P, Gentine P, Jung M, Reichstein M, Seneviratne S I and Frankenberg C 2021 Soil moisture–atmosphere feedback dominates land carbon uptake variability *Nature* **592** 65–69
Ibrahim Y Z, Balzter H, Kaduk J and Tucker C J 2015 Land degradation assessment using residual trend analysis of gimms ndvi3g, soil moisture and rainfall in sub-saharan west africa from 1982 to 2012 *Remote Sens.* **7** 5471–94
Ingeri C, Wen W, Sebaziga J N, Iyakaremye V, Ekwacu S, Ayabagabo P, Twahirwa A and Kazora J 2024 Potential driving systems associated with extreme rainfall across East Africa during october to december (ond) season 2019 *J. Geosci. Environ. Protect.* **12** 25–49
Kayiranga A, Chen B, Wang F, Nthangeni W, Dilawar A, Hategekimana Y, Zhang H and Guo L 2022 Spatiotemporal variation in gross primary productivity and their responses to climate in the great lakes region of sub-Saharan Africa during 2001–2020 *Sustainability* **14** 2610
Kooistra L *et al* 2024 Reviews and syntheses: remotely sensed optical time series for monitoring vegetation productivity *Biogeosciences* **21** 473–511
Küllahcı K and Altunkaynak A 2024 Maximizing daily rainfall prediction accuracy with maximum overlap discrete wavelet transform-based machine learning models *Int. J. Climatol.* **44** 3405–26
Lee H *et al* 2023 IPCC *2023: Climate Change 2023: Synthesis Report, Summary for Policymakers. Contribution of Working Groups i, ii and iii to the Sixth Assessment Report of the Intergovernmental Panel on Climate Change [Core Writing Team, h. lee and j. Romero (eds.)]* (IPCC) pp 35–115
Liu J *et al* 2017 Contrasting carbon cycle responses of the tropical continents to the 2015–2016 el niño *Science* **358** eaam5690
Liu Y, Liu Y, Wang W, Fan X and Cui W 2022 Soil moisture droughts in east africa: Spatiotemporal patterns and climate drivers *J. Hydrol. Reg. Stud.* **40** 101013
MacLeod D and Caminade C 2019 The moderate impact of the 2015 el niño over East Africa and its representation in seasonal reforecasts *J. Clim.* **32** 7989–8001
McKee T B *et al* 1993 The relationship of drought frequency and duration to time scales *Proc. 8th Conf. on Applied Climatology* vol 17 pp 179–83
Meng M, Huang N, Wu M, Pei J, Wang J and Niu Z 2019 Vegetation change in response to climate factors and human activities on the mongolian plateau *PeerJ* **7** e7735
Mondal S and Vivoni E R 2025 Hot drought of summer 2023 in Southwestern North America *Geophys. Res. Lett.* **52** e2025GL118308
Muñoz Sabater J 2019 ERA5-land monthly averaged data from 1981 to present, Copernicus Climate Change Service (C3S) Climate Data Store (CDS) *Earth Syst. Sci. Data* **55** 5679
Muñoz Sabater J *et al* 2021 ERA5-land: a state-of-the-art global reanalysis dataset for land applications *Earth Syst. Sci. Data Discuss.* **13** 1–50
Nhamo L, Mpandeli S, Liphadzi S, Dirwai T L, Mugiyo H, Senzanje A, Lankford B A and Mabhaudhi T 2024 Why do farmers not irrigate all the areas equipped for irrigation? lessons from southern africa *Agriculture* **14** 1218
Nicholson S E 2014 A detailed look at the recent drought situation in the greater horn of africa *J. Arid Environ.* **103** 71–79
Nicholson S E 2017 Climate and climatic variability of rainfall over eastern africa *Rev. Geophys.* **55** 590–635
Palmer P I *et al* 2023 Drivers and impacts of eastern african rainfall variability *Nat. Rev. Earth Environ.* **4** 254–70
Percival D B and Walden A T 2000 *Wavelet Methods for Time Series Analysis* vol 4 (Cambridge)
Pettorelli N, Vik J O, Mysterud A, Gaillard J M, Tucker C J and Stenseth N C 2005 Using the satellite-derived ndvi to assess ecological responses to environmental change *Trends Ecol. Evol.* **20** 503–10
Pettorelli N, Vik J O, Mysterud A, Gaillard J-M, Tucker C J and Stenseth N C 2005 Using the satellite-derived ndvi to assess ecological responses to environmental change *Trends Ecol. Evol.* **20** 503–10
Phiri M, Shiferaw Y A and Tesfamichael S G 2018 Modelling the relationship between groundwater depth and ndvi using time series regression with distributed lag M *South African J. Geom.* **7** 147–63
Plisnier P-D *et al* 2023 Need for harmonized long-term multi-lake monitoring of african great lakes *J. Gt. Lakes Res.* **49** 101988
Qu C, Hao X and Qu J J 2019 Monitoring extreme agricultural drought over the horn of africa (hoa) using remote sensing measurements *Remote Sens.* **11** 902
Raghuraman S P, Soden B, Clement A, Vecchi G, Menemenlis S and Yang W 2024 The 2023 global warming spike was driven by the el niño–Southern Oscillation *Atmos. Chem. Phys.* **24** 11275–83
Rahimabadi P D and Azarnivand H 2023 Assessment of the effect of climate fluctuations and human activities on vegetation dynamics and its vulnerability *Theor. Appl. Climatol.* **153** 771–86
Runge J *et al* 2019 Inferring causation from time series in earth system sciences *Nat. Commun.* **10** 1–13
Saji N H, Goswami B N, Vinayachandran P N and Yamagata T 1999 A dipole mode in the tropical indian ocean *Nature* **401** 360–3
Sato H and Ise T 2012 Effect of plant dynamic processes on african vegetation responses to climate change: analysis using the spatially explicit individual-based dynamic global vegetation model (SEIB-DGVM) *J. Geophys. Res.* **117** G03017
Singh A, Diop S and M'mayi P L 2006 *Africa's Lakes: Atlas of Our Changing Environment* (United Nations Environment Programme)
Sogno P, Klein I, Uereyen S, Bachofer F and Kuenzer C 2024 Surface water dynamics of africa: analysing continental trends and identifying drivers for major lakes and reservoirs *Int. J. Remote Sens.* **45** 9538–68
Staal A, Tuinenburg O A, Bosmans J H, Holmgren M, van Nes E H, Scheffer M, Zemp D C and Dekker S C 2018 Forest-rainfall cascades buffer against drought across the amazon *Nat. Clim. Change* **8** 539–43
Tall M *et al* 2023 Drought variability, changes and hot spots across the african continent during the historical period (1928–2017) *Int. J. Climatol.* **43** 7795–818
Thielke A and Mölg T 2019 Observed and simulated indian ocean dipole activity since the mid-19th century and its relation to east african short rains *Int. J. Climatol.* **39** 4467–78
Torrence C and Compo G P 1998 A practical guide to wavelet analysis *Bull. Am. Meteorol. Soc.* **79** 61–78
Tucker C J 1979 Red and photographic infrared linear combinations for monitoring vegetation *Remote Sens. Environ.* **8** 127–50
Wainwright C M, Marsham J H, Keane R J, Rowell D P, Finney D L, Black E and Allan R P 2019 Eastern African paradox' rainfall decline due to shorter not less intense long rains *npj Clim. Atmos. Sci.* **2** 34
Wessels K J, Van Den Bergh F and Scholes R 2012 Limits to detectability of land degradation by trend analysis of vegetation index data *Remote Sens. Environ.* **125** 10–22
Wigneron J-P, Fan L, Ciais P, Bastos A, Brandt M, Chave J, Saatchi S, Baccini A and Fensholt R 2020 Tropical forests did not recover from the strong 2015–2016 el niño event *Sci. Adv.* **6** eaay4603
Wilks D S 2011 *Statistical Methods in the Atmospheric Sciences* 3rd edn vol 100 (*International Geophysics Series*) (Academic)
Wright A J 2024 Plant–plant interactions can mitigate (or exacerbate) hot drought impacts *New Phytol.* **241** 955–7

Wuestenberg A, Dujanovic D and Parodi L 2016 *Global Early Warning – Early Action Report on Food Security and Agriculture October - December 2016* FAO pp 28 (available at: https://openknowledge.fao.org/server/api/core/bitstreams/43ffc3f8-d66b-4333-a042-128826f48e60/content)

Xu M, Zhang Z, Wang Y and Liu B 2024 Quantifying the contributions of climatic and human factors to vegetation net primary productivity dynamics in east africa *Front. Forests Glob. Change* **6** 1332631

Zeraati M, Farahmand A, Asghari K and Behrangi A 2024 Developing a multivariate agro-meteorological index to improve capturing onset and persistence of droughts utilizing vapor pressure deficit and soil moisture *Earth Space Sci.* **11** e2023EA003273

Zhou L *et al* 2014 Widespread decline of congo rainforest greenness in the past decade *Nature* **509** 86–90

Zhu Z *et al* 2016 Greening of the earth and its drivers *Nat. Clim. Change* **6** 791–5

Zita L E, Justino F, Gurjão C, Adamu J and Talacuece M 2025 Spatio-temporal characteristics of climate extremes in sub-saharan africa and potential impact of oceanic teleconnections *Atmosphere* **16** 86